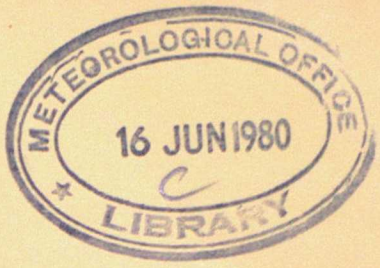

METEOROLOGICAL OFFICE
RADAR RESEARCH
LABORATORY

RSRE MALVERN ENGLAND

RESEARCH REPORT

No. 17

April 1980

An observational study of primary and secondary billows in the free atmosphere

by

P K James and K A Browning

Meteorological Office Radar Research Laboratory,

Royal Signals and Radar Establishment,

Malvern, Worcs.

SUMMARY

A case study is presented showing the kinematic structure of a train of large-amplitude billows associated with a strongly sheared layer of high static stability in the upper troposphere. The observations were obtained using a high-power microwave Doppler radar with a range resolution of 30 m. A beamwidth resolution almost as good as this was achieved at the ranges of interest using a 25 m paraboloid aerial. The resulting detailed measurements revealed the kinematic structure of secondary billows of wavelength 350 m growing on the back of primary billows of wavelength 4.2 km. The secondary billows were regions of moderate turbulence, the outer scale of which was small compared with the radar resolution. Streamers of cirrus ice particles were present in the region of interest and these served as tracers showing how the billows perturbed the flow over a considerable depth above and below the billows.

1 Introduction

In this paper we present Doppler radar observations of the airflow within billows that were responsible for patches of moderately intense turbulence within a strongly sheared layer in the free atmosphere. Radar has an advantage over direct probing techniques in that it can provide velocity measurements at many altitudes simultaneously and so it can be used to depict vertical structure on a continuous basis. However, two disadvantages of radar in this kind of study are usually its poor spatial resolution and the fact that the natural radar targets required to trace the airflow are often not conveniently distributed over the entire depth of interest. In this study both these disadvantages have been partly overcome, with the result that an unusually complete description of the kinematics of a train of atmospheric billows has been achieved. The observations are of interest since they reveal the effect of the primary billows in perturbing a fairly deep layer in which they were embedded and also since they reveal the structure of smaller secondary billows formed in regions where the primary billows were concentrating the vertical wind shear.

The radar used in this study was the large high-power 10 cm wavelength system at RSRE Defford (Watkins 1971). This was first used as a conventional (non-Doppler) radar with 200 m range resolution to study the occurrence (Browning 1971) and evolution (Browning and Watkins 1970) of large-amplitude billows in relation to the vertical structure of the atmosphere as determined from serial radiosondes. The presence and broad structure of the billows was inferred from the characteristic breaking-wave patterns of the clear air returns obtained from refractive index inhomogeneities (as first reported by Hicks and Angell 1968).

The Defford radar was subsequently converted for use as a pulsed Doppler radar - still with 200 m range resolution - to measure the coarse kinematic

features of large-amplitude billows (Browning et al.1972). In another study (Browning et al. 1973), the Doppler radar observations were complemented by simultaneous measurements from an instrumented aircraft. This showed a good relationship between the primary billow echoes and clear air turbulence detected by the aircraft (see also Browning et al.1970; Hardy et al. 1973). However, in addition to the bursts of turbulence associated with the primary billows of wavelength 2 km, Browning et al.(1973) noted that the aircraft encountered turbulence bursts which 'appeared to be associated with secondary billows of wavelength 600 m whose amplitude was too small ($\sim$100 m) to be adequately resolved by the radar'.

Since the time of the above studies, the Doppler radar at Defford has been substantially rebuilt by RSRE personnel (Whyman and Parkes 1979). In its new form the radar utilises pulse compression techniques to give a range resolution of 30 m, almost an order of magnitude better than before. Together with a good ($\frac{1}{3}^{o}$)angular resolution achieved with the 25 m diameter aerial, this makes the Defford Doppler radar well-suited to observing the smaller scale secondary billows referred to above. FM-CW Doppler radars* are also well equipped to resolve fine scale features (Chadwick et al.1976) but these radars tend to be limited to maximum ranges of less than 3 km, thus are not as suitable as pulsed Doppler radars for studying atmospheric structure above the disturbed boundary layer.

The observations described in this paper were obtained with the new Doppler radar at Defford on 30 March 1977 when a train of large-amplitude billows passed over the radar at an altitude of 7 km. The observations have already been reported in a brief letter to Nature (Browning et al.1978) as an

---

*Non-Doppler FM-CW radars can resolve scales down to a few metres - see, for example, Fig 12 of Gossard et al.(1971)which shows billows of 5 m amplitude outlining a larger gravity wave disturbance.

example of the use of the upgraded Defford radar, but the analysis will now be taken much further to provide meteorological insight into the structure and mechanism of the billows. This has been a rewarding case for study because small cirrus ice particles provided tracers of the air motion over a layer far deeper than that provided by the clear air returns used in most previous radar investigations of billows. Fortunately the ice particles were in the form of discrete streamers whose slope was distorted by the billows: if there had been a more uniform zone of ice particles, all trace of billow perturbation would have been obliterated from the reflectivity pattern detected by the radar.

A word of explanation is called for over our use of the terminology 'primary' and 'secondary' as applied to billows. We use the term primary to denote the billows of longer wavelength and dominant amplitude. The secondary billows discussed in this paper developed within the primary billows when the latter attained the largest observed amplitude. For this reason it is considered that the amplification of the primary billows was leading to the development of the secondary instabilities. These evolved on the sloping surfaces of the larger billows probably in the manner suggested by Scorer (1979) and Ottersten (1970). However, this is not to deny the existence of some 'mini' billows even before the development of the main billows - a fact which led Atlas and Metcalf (1970) to adopt the different convention of referring to mini billows as the primary billows because of the temporal precedence of the mini billows in their study.

According to Scorer (1978), the life cycle of billows involves the rolling up of a dynamically unstable shear layer; the fluid in the rolls is then convectively unstable and mixes turbulently. In the present study the secondary billows were observed at a time when the primary billows had not advanced very far in such a roll-up process. Most of the turbulence in the present case is believed to have been associated with the secondary billows.

2. The synoptic setting for the case study

The large-amplitude billow event was observed over Defford, Worcs ($52^{\circ}6'$ N, $2^{\circ}9'$W) between 1440 and 1505 GMT on 30 March 1977. Five radiosondes were released from Defford between 1210 and 1745 GMT. During this period Defford was on the NE flank of an upper tropospheric jet stream which was blowing from 330° with a jet maximum of about 75 ms^{-1} at 11.4 km. Fig 1(a) is a vertical section across the jet axis showing the component of the wind from 330° as measured by routine radiosondes at 12 GMT plus one at Defford. The winds were within $\pm 10^{\circ}$ of this direction over the entire layer occupied by the billows. Fig. 1(b) is a time-height section showing the same wind component as measured at Defford, the equivalent distance scale being calculated using the speed of travel of the synoptic scale pattern. The billow event is marked in Fig 1(b), from which it is clear that it occurred in a region where the vertical wind shear attained a maximum value on the mesoscale. Fig 1(b) also shows that the billow event occurred near the top of a cirrus cloud layer; the radiative cooling at the top of this cloud may have contributed to the destabilisation of the layer.

The 1450 GMT radiosonde from Defford showed a strongly sheared layer of high static stability at the level of the billows. At 6.8 km the wind was $320^{\circ}/18$ ms^{-1} and at 7.7 km it was $338^{\circ}/40$ ms^{-1}. Fig 2 shows vertical profiles of the vertical gradient of dry bulb potential temperature, the magnitude of the vector wind shear and the Richardson number, all evaluated over height intervals of 430 m. Both the shear and the Richardson number varied considerably with height in the vicinity of the billow event. This may have been because the radiosonde ascended through the region recently disturbed by the billows. The Richardson number in this region is seen to have been close to the value of $\frac{1}{4}$ regarded as the critical value for the onset of shearing instability. (Miles and Howard 1964).

3. The basic Doppler radar observations

The characteristics of the upgraded Defford radar are outlined in Appendix 1 along with a description of the methods of recording the data and processing them to extract the main properties of the Doppler spectra (ie reflectivity η, mean radial velocity V_r and velocity variance σ^2_v within each resolution cell). Suffice it to mention here that the radar can be thought of as having a resolution cell of 30 x 45 x 45 m at the ranges of interest and enough sensitivity to detect the very small ice crystals that were present in the region of the billows. During the observational period the radar beam was fixed in a direction of 330° and at an elevation of 60°. The azimuth was chosen to be close to both the mean wind ($330 \pm 5^\circ$) and the wind shear vector ($350 \pm 8^\circ$) over the layer of the billows. The elevation angle of 60° was a compromise between the need for a high elevation to achieve a nearly vertical sounding and an elevation low enough to detect a large component of the vertical shear of the horizontal wind.

Observations of radar reflectivity were obtained on a photographic strip chart recorder over ranges corresponding to the height interval 4.7 to 10.5 km. The record from 1446 to 1458 GMT (Fig 3) shows streamers of ice crystals whose slope is distorted by a wavelike disturbance with a period of about 160s in the sheared layer between 6.0 and 7.7 km. Thirty contiguous 30 m range gates located at heights between 6.75 and 7.53 km were selected for more detailed processing using 1-sec portions of data at 3-sec intervals over the interval 1440 to 1454 GMT. The resulting patterns of V_r and σ^2_v are plotted in a time-range format in Figs 4 and 5. Also shown in the same format (Fig 6) is the radial shear $\left(\frac{\Delta Vr}{\Delta r}\right)$ evaluated as the difference in radial velocity between range gates whose mid-points were 60 m apart in range. (The pattern of shear in this figure is smoother and more coherent than in the preliminary analysis reported by Browning et al.(1978). This is because a more elaborate method of data

processing was used (Appendix 1) which enabled V_r to be estimated to the nearest 0.1 ms^{-1}, almost an order of magnitude better than in the previous analysis).

The wavelike disturbance evident in Fig 3 is clearly indicated in the distortion of the contours of V_r, σ_V^2 and $\frac{\Delta Vr}{\Delta r}$ in Figs 4, 5 and 6. At 1436 GMT, before the disturbance had begun to develop, Doppler measurements (not illustrated) indicated a vertical wind shear of 2.7×10^{-2} s^{-1} in the height interval 6.75 to 7.15 km. This compared well with the magnitude of the shear estimated from the nearby radiosonde (Fig 2). After 1445 GMT when the billows were well-established the shear became concentrated into a thinner waving layer. The axis of the undulating layer of maximum shear (Fig 6) corresponds closely to the location of the thin layer of large σ_V^2 (Fig 5). Another feature of the wind shear pattern that was modulated by the billows was a thin layer of reversed or low shear just above the main shear layer. Although less than 60 m deep and having a velocity decrement of at most 0.15 ms^{-1} across it, this layer preserved its identity for the entire period of observation (being represented in Fig 6 by the dashed line).

4. Structure of the primary billows

The radar data presented above were collected in a time-range format. In order to obtain a picture of the spatial structure of the billows, however, it is necessary to make some assumptions about the billows themselves. The major assumption is that each primary billow retained a steady state structure during the 160 seconds it took to pass over the radar. The velocity of propagation of the billows is taken to be equal to the mean wind in the strongly sheared layer, namely 26 m s^{-1}, and this gives a wavelength of 4.2 km for the billows. We know from previous studies of the evolution of billows of similar size that significant amplification can occur within 160 seconds (Browning and Watkins 1970); nevertheless their wavelength remains fairly constant and the rate of amplification is not

thought to be so great as to render the use of the steady state assumption meaningless. Since the small ice particles detected by the radar in the present study provided good tracers of the flow, the use of the steady state assumption has enabled us to derive an approximate streamline pattern relative to the primary billows, with the results shown in Figure 7(b).

A pattern velocity of 26 ms^{-1} has been used in the derivation of this figure, not only to give the equivalent distance scale, but also to compensate for the 60° elevation angle of the radar beam. Thus the vertical axis in Fig 7(b) is to be interpreted simply as height vertically above the radar instead of height along the axis of the beam as is the case for the basic data in Figs 3 to 6.

The strands of evidence exploited in deriving the streamlines in Fig 7(b) are as follows:-

All the streamlines except those labelled (1) and (2) were derived from the shape of the ice crystal trails after making allowance for their average slope.

The streamline labelled (1) has been drawn to correspond to the layer of reversed or minimum shear (dashed curve in Fig 6) assuming that to a first approximation this very shallow layer served as a passive tracer of the flow.

The streamline labelled (2) has been drawn to correspond to the axis of maximum shear and the closely associated maximum of velocity variance (Figs 6 and 5). Again we are assuming that the developing billows were distorting a pre-existing shear layer. However, we know that the billows were also concentrating the shear and, to the extent that the redistribution of shear may have been different in different parts of each billow, then the inferred shape of streamline (2) would be in error. Since this streamline does appear to be consistent with the form of the

reflectivity pattern, we consider the streamline not to be grossly in error.

The most striking feature of the flow pattern depicted in Fig 7(b) is the change in phase with height: the wave crests are displaced in the downshear direction, the topmost parts being almost in antiphase with the lowest parts at 1454 GMT. Such a pattern is characteristic of billows (Scorer 1978), the layer of maximum shear (streamline (2)) corresponding to a critical layer (Gossard and Hooke 1975, p 170). The amplitude of such a disturbance is likely to be greatest at the critical level (Barcilon and Lessen 1978). The crest-to-trough amplitude of streamline (2) between 1448 and 1455 GMT was 340 m. The amplitude of the disturbance decreased to half this value at distances of 550 m above and below the critical layer.

Although our assumption of steady state conditions is unlikely to be rigorously applicable, we do not consider that the gross features of the flow pattern, namely the wavelength, amplitude and the phase change with height, are seriously in error.

We remarked earlier about the presence of a layer of reversed or minimum shear less than 60 m deep, situated above the strongly sheared layer (i.e. streamline (1) in Fig 7(b)). This layer was present both at the time of the billows and before they developed. It was therefore not an effect due to the billows themselves but was perhaps due to a mesoscale disturbance (which may have been the disturbance responsible for redistributing the shear and triggering the major billow event in the first place). Shallow layers of reversed shear - one above and another below a strongly sheared layer in which billows developed - have been observed by Browning (1971) who drew attention to the associated looped hodograph. Unfortunately, in the present study radiosonde data were not accurate enough to resolve such details and the Doppler data did not extend low enough to enable us to determine whether there was another layer of reversed shear below the billows.

The velocity information plotted earlier in Fig 4 was the radial velocity (Vr) along the 60° axis of the radar beam. In order to separate the horizontal and vertical velocity contributions, we have integrated the 2-dimensional continuity equation for an incompressible fluid using streamline (1) as a boundary condition. Again, we have assumed steady state conditions. The computed vertical velocity (not shown) reaches values of 0.8 to 1.3 ms^{-1} just above and below the undulating critical layer. Even as far as 500 m above this layer the vertical velocity occasionally reached $\pm$1.0 ms^{-1}. (This was because, although the amplitude of the billows decreased with distance from the critical level, the wind speed relative to the pattern was proportionately greater). The values of horizontal wind speed estimated using continuity considerations have been used to derive the pattern of vertical shear of the horizontal wind and a simplified version of this is plotted in Fig 7(c) in the same rectified height-time format as Fig 7(b). Before 1441 GMT (not shown) the vertical wind shear had been spread over a layer about 400 m deep and it averaged 2.7 x $10^{-2}s^{-1}$. By 1449, however, the shear was concentrated into a waving layer only about 150 m thick, the average vertical shear across this layer having increased to 4.8 x $10^{-2}s^{-1}$. The wavelength (λ) of the primary billow, 4.2 km, was evidently about 10 times greater than the thickness (h) of the undisturbed shear layer before 1441. Theoretical treatments give values of 5 to 9 for the ratio λ/h (Gossard and Hooke 1975).

The observed variance of the Doppler spectra σv^2, plotted earlier in Fig. 5, represents the sum of contributions due to the radial and transverse shear of the radial velocity, the fall speed distribution of the ice crystals resolved along the radial direction, the turbulence on scales smaller than the pulse volume, a beamwidth broadening effect associated with the radial components of the tangential wind at the edges of the radar beam (Hitschfeld and Dennis 1956) and an instrumental contribution, i.e.

$$\sigma_v^2 = \sigma_{RSH}^2 + \sigma_{TSH}^2 + \sigma_{FALL}^2 + \sigma_{TURB}^2 + \sigma_{BW}^2 + \sigma_{INST}^2$$

The variance σ^2_{INST} is less than 0.1 $m^2 s^{-2}$. With a narrow ($\frac{1}{3}^o$) beam, the variance σ^2_{BW} is also negligible. In regions away from the strongly sheared layer the values of σ^2_v are attributable mainly to the fall speed distribution of the ice crystals (σ^2_{FALL}). Since these values were as small as 0.1 to 0.2 m^2 s^{-2}, it is evident that σ^2_{FALL} will have made only a minor contribution in the strongly sheared regions where σ^2_v was commonly in excess of 1 $m^2 s^{-2}$. Now, the variance due to radial and transverse shear can be calculated directly from the data in Fig 4 (Strauch et al 1975), and so the variance due to turbulence on scales smaller than the pulse volume (σ^2_{TURB}) can be estimated as a residual. The resulting pockets of intense turbulence have been plotted in Fig 7(c), from which it can be seen that nearly all the regions where $\sigma^2_{TURB} > 2$ $m^2 s^{-2}$ were located within the strongly sheared layer. Maximum values of σ^2_{TURB} were close to 3.0 $m^2 s^{-2}$. The largest values of σ^2_{TURB} had a tendency to occur in the parts of the billows inclined in the same sense as the vertical shear vector and tended to be associated with the formation of secondary billows the structure of which is discussed in the next section.

5. Structure of the secondary billows

During the early stages of the observed passage of the primary billows the isotach pattern varied quite smoothly, with a period of about 160s (see parts of the record in Fig 4 before 1445 GMT). Subsequently, perturbations in velocity developed which passed through the radar beam at 14s intervals (see the part of the record in Fig 4 between 1453 and 1454 GMT). These same perturbations also gave rise to corrugations in the reflectivity distribution (see Fig 3). The perturbations are thought to have been due to small scale (secondary) billows growing on the back of the amplifying primary billows. Since they developed within the same strongly sheared layer that was being distorted by the primary billows, it is assumed they travelled with the same velocity (26 ms^{-1}) as the train of primary billows. This implies a wavelength of 350 m for the secondary billows compared with 4.2 km for the primary billows.

In order to analyse the fine scale structure of these billows we shall avoid the complexities of the series of vigorous secondary billows between 1453 and 1454 GMT and, instead, concentrate on a more isolated secondary billow which occurred at 1451½ GMT. The region involved is denoted by the small rectangle in Figs 7(b) and (c). In this region the Doppler spectra for individual pulse volumes, plotted in Fig 8, instead of being Gaussian as assumed in the simple analysis in Sec. 3 (see Appendix 1), were occasionally multipeaked. Distinct velocity peaks up to 2.4 ms^{-1} apart indicated the existence of quite large velocity differences within individual pulse volumes. Accordingly, we have derived the detailed kinematic structure in this region manually by reference to the raw Doppler spectra. (Where two widely spaced peaks occur within a single spectrum, the velocity contours have been drawn to be consistent with both velocities being present in the corresponding pulse volume separated by a strong gradient). The resulting kinematic structure of this secondary billow is shown in Fig 9, in which the patterns have been rectified to give a true cross-sectional representation as in Fig 7.

Fig 9(a) depicts isopleths of radial velocity (v_r) contoured from an array of 54 data points. Notice the greater amount of fine scale structure than revealed by the simpler analysis in the corresponding part of Fig 4. Fig 9(b) depicts the vertical velocity derived from the continuity equation as described in the previous section. Notice the well-defined up-down doublet with ascent in excess of 2 m s^{-1} near X and descent in excess of 1 m s^{-1} at Y. This is attributed to the effect of the secondary billow with vertical velocity $\pm$ 1½ ms^{-1} being embedded in the upslope portion of the primary billow characterised by general ascent of about ½ ms^{-1}. The horizontal spacing of the upward (X) and downward (Y) parts of the secondary billow corresponds to the 350 m wavelength of this disturbance. The flow visualisation, derived by eye from Figs 9(a) and (b), is sketched in Fig 9(c).

Fig 9(d) depicts the residual variance (σ^2_{TURB}) due to turbulence in the vicinity of the secondary billow, derived from the observed variance of the Doppler spectra by subtracting out the effects of larger-scale shear in the manner described in the previous section. Notice how the maximum value of σ^2_{TURB} was associated with the strongly bimodal spectrum marked * in Fig 8 and with the contorted isotaches in Fig 9(a). Several of the spectra had multiple peaks in this region, and although this could have been partly due to non-uniformity in the distribution of ice crystal targets, it is more likely to be an indication that the outer scale of the turbulence was small compared with the pulse volume. Thus the derived values of variance for the 'turbulence' in this region represent the combined effect of random turbulence together with more organised motions occurring on a very small scale (tertiary billows?). This is reminiscent of the observations by Metcalf and Atlas (1973) of a thin statically stable layer in which well ordered motions were found down to scales as small as a few metres or less.

Frisch and Clifford (1974) have given a relationship between the turbulent dissipation rate ϵ and σ^2_{TURB} on the assumption that the outer scale of the inertial subrange is larger than the radar pulse volume. Although this is a poor assumption on this occasion, if we tentatively apply Frisch and Cliffords' relationship we would infer peak values of ϵ of about 2500 $cm^2 s^{-3}$. According to MacCready (1964) and Trout and Panofsky (1969) this would be sensed by an aircraft as severe turbulence. Taking into account the inadequacy of the above assumption, it seems more reasonable to assume that the 'turbulence' in the present case would have been sensed as more or less moderately intense depending on the type of aircraft encountering it.

6. Conclusions

High-resolution measurements with a 10 cm wavelength Doppler radar have been analysed to show the structure of a train of billows associated with the

strongly sheared lower boundary of an upper tropospheric jet stream. The relatively detailed measurements enabled small secondary billows to be observed growing on the back of the primary billows. The secondary billows had a wavelength of 350 m and crest-trough amplitude of 50 m, compared with values of 4.2 km and 340 m, respectively, for the parent billows.

The maximum velocity variance, due to turbulence and other more organised velocity changes within an individual radar pulse volume, was observed to be over 3 $m^2 s^{-2}$. The distribution of 'turbulence' measured by the radar was very patchy; all the resolved secondary billows gave rise to pockets of intense turbulence. The outer scale of this turbulence was small compared with the radar pulse volume (30 x 45 x 45 m). In other words we have found the turbulence to be anisotropic on scales of 30 m in billows of wavelength 4.2 km: by comparison Metcalf and Atlas (1973) have found that in 80 m wavelength billows the turbulence can be anisotropic down to a scale of about 1 m.

The presence of streamers of cirrus ice crystals provided tracers which enabled the air motion to be observed over a layer extending some distance above and below the strongly sheared layer. It was found that the amplitude of the primary flow perturbation exceeded half its peak amplitude over a depth of 1100 m. The depth of the shear layer itself was much less than this. Before the onset of the instability, it was only 400 m deep, the shear averaging $2.7 \times 10^{-2} s^{-1}$ over this height interval. When the primary billows developed, the shear layer became concentrated in a layer between 100 and 200 m thick. In parts of the primary billows, including the regions where secondary billows were observed, the vertical shear evaluated over 50 m intervals became as large as $6 \times 10^{-2} s^{-1}$.

APPENDIX 1

The Doppler radar and basic data processing

The radar at Defford, Worcestershire, has been designed to achieve high spatial resolution and great sensitivity. The 107 mm wavelength radar (an FPS-18 on loan from the National Center for Atmospheric Research) is coupled to a 25 m diameter aerial to give an angular beam-width of $\frac{1}{3}^{\circ}$. The radar transmits frequency-modulated pulses of length 600 m. After reflection from targets these pulses are received, compressed and range-gated to give a resolution of 30 m.

The high gain of the aerial, low receiver noise and compression combine to produce the high sensitivity. The minimum detectable reflectivity (without integration) for an extended target is 1.2×10^{-15} m^{-1} at a range of 5 km. A phase sensitive detector output from the receiver gives the in-phase component of the Doppler frequency. Since returns from the ground, received in the aerial side-lobes, are at least as large as those from wanted targets, a range gated MTI (moving target indicator) is used to filter out the stationary targets. The MTI can handle 256 contiguous gates, each 30 m wide, covering a total range interval of 7.5 km which can be set anywhere between 0 and 100 km. The output of the MTI is displayed on a photographic strip chart to produce an intensity modulated time-range record of target reflectivity. Doppler information from 30 selected range gates covering a total range interval of 900 m is recorded on audio tape. This can be replayed and frequency spectrum analysed to give the Doppler velocity unambiguously over the range 0 to 25 ms^{-1}. If other batches of 30 range gates need to be processed similarly they can be extracted from a video recording of the raw radar data.

Spectrum analysis is performed off-line by a hardwired Fast Fourier Transform processor controlled by a minicomputer. The analogue signal from each of the range gates recorded on the audio tape is sampled and digitised at

at 1024Hz. A total of 1024 consecutive numbers are Fourier Transformed and then processed to give 512 numbers each proportional to the logarithm of the power in consecutive 1 Hz intervals of frequency. These numbers are stored on digital magnetic tape for analysis on an ICL 1906S mainframe computer. The 512-word spectra are analysed to give estimates of the mean Doppler velocity, peak velocity variance, peak power and background noise.

A significant proportion of the spectra had very small peak signals, and as a result conventional methods of estimating spectral parameters proved unreliable. The current results were obtained by a least squares fit to the logarithmic power spectrum of the logarithm of the Gaussian function:

$$F(v_r) = \ell n \left[a_s \exp\left\{ -\tfrac{1}{2} \left(\frac{V_r - V_{ro}}{v} \right)^2 \right\} + 1 \right] + \ell n \left[a_n \right] \quad \ldots \quad A1$$

where V_r is the Doppler velocity, V_{ro} is the peak centre velocity, σ_v is the peak standard deviation. $\ell n \left[a_n \right]$ is the noise in dB and $\ell n \left[a_s + 1 \right]$ is the height of the peak above noise in dB. The use of the logarithm of a Gaussian allows errors in the power in the observed spectra to be assigned as $\pm$ xdB in the fitting procedure. This particular process was adopted because it has a high immunity to noise well away from the observed mean velocity. The least-squares fitting procedure used the Marquardt (1963) gradient-expansion algorithm as described by Bevington (1969). This method relies on the observed spectra being Gaussian. If the reflected signal is predominantly from ice particles distributed uniformly across the pulse volume, then linear shear would give a Gaussian contribution to the Doppler spectrum by virtue of the Gaussian distribution of transmitter power across and along the pulse volume. The fall speed distribution of ice particles is not necessarily Gaussian but the contribution of this to the total variance was small in the present study (< 0.5 m^2 s^{-2}). Turbulence with an outer scale smaller than the pulse volume sometimes gave a large and markedly non-Gaussian contribution; in such cases the fitted spectra were inspected by eye and those which appeared to be a poor fit were analysed manually.

REFERENCES

Atlas D. and Metcalf J I., 1970 : The amplitude and energy of breaking Kelvin-Helmholtz waves and turbulence. Technical Report No.19, Laboratory for Atmospheric Probing, The University of Chicago.

Barcilon A. and Lessen M., 1978 : On the splitting of atmospheric and oceanic turbulent billows. Tellus 30 pp 557-561

Bevington P.R., 1969 : Data reduction and error analysis for the physical sciences. McGraw-Hill, New York.

Browning K.A., 1971 : Structure of the atmosphere in the vicinity of large-amplitude Kelvin-Helmholtz billows. Quart. J. Roy. Met. Soc., 97, pp 283 - 299.

Browning K.A., Bryant G W., Starr, J R, and Axford, D N., 1973 : Air motion within Kelvin-Helmholtz billows determined from simultaneous Doppler radar and aircraft measurements. Quart. J. Roy. Met. Soc., 99 pp 608-618.

Browning K.A., James P K., Parkes D M., Rowley C., and Whyman A J., 1978 : Observations of strong wind shear using pulse compression radar. Nature 271 pp 529 - 531.

Browning K.A., Starr J R., and Whyman A J., 1972 : Measurements of air motion in regions of clear air turbulence using high power Doppler radar. Nature 239 pp 267 0 269.

Browning K.A., and Watkins C.D., 1970 : Observations of Clear Air Turbulence by High Power Radar, Nature, 227 pp 260-263.

Browning K.A., Watkins C.D., Starr J.R., and McPherson A., 1970 : Simultaneous measurements of clear air turbulence at the tropopause by high-power radar and instrumented aircraft. Nature 228 pp 1065-1067.

Chadwick R.B., Moran K.P., Strauch R.G., Morrison G.E and Campbell W.C., 1976 : A new radar for measuring winds. Bull. Amer. Met. Soc. 57 pp 1120-1125.

Frisch A.S. and Clifford S.F., 1974 : A study of convection capped by a stable layer using Doppler radar and acoustic echo sounders. J.Atmos. Sci. 31 pp 1622 - 1628.

Gossard E.E. and Hooke W.H., 1975 : Waves in the Atmosphere. Elsevier Scientific Publishing Co., Amsterdam.

Gossard E.E., Jensen D.R. and Richter J.H., 1971 : An analytical study of tropospheric structure as seen by high-resolution radar. J.Atmos. Sci. 28 pp 794 - 807.

Hardy K.R., Reed R.J., and Mather G.K., 1973 : Observations of Kelvin-Helmholtz billows and their mesoscale environment by radar, instrumented aircraft, and a dense radiosonde network. Quart. J.Roy. Met. Soc. 99 pp 279 - 293.

Hicks J.J. and Angell J.K., 1968 : Radar observations of breaking gravitational waves in the visually clear atmosphere. J. Appl.Meteor. 7 pp 114-121.

Hitschfeld W and Dennis A.S., 1956 : Turbulence in snow generating cells. Sci. Report. MW-23, 31 pp McGill University, Montreal, Canada.

MacCready P.B., 1964 : Standardization of gustiness values from aircraft. J. Appl. Met., 3 pp 439-449.

Marquardt D.W., 1963 : An Algorithm for Least-Squares Estimation of Non-linear Parameters. J. Soc. Ind. Appl. Math. 11 pp 431 - 441.

Metcalf J.I. and Atlas D., 1973 : Microscale ordered motions and atmospheric structure associated with thin echo layers in stably stratified zones, Boundary-Layer Met., 4 pp 7 - 35.

Miles, J.W., and Howard L.N., 1964 : Note on heterogeneous shear flow. J. Fluid Mech. 20 pp 331 - 336.

Ottersten H.,1970 : Radar Observations of the Turbulent Structure in Shear Zones in the Clear Atmosphere. Preprints 14th Radar Meteorology Conference, Tucson. American Met. Soc., pp 111 - 116.

Scorer R.S., 1969 : Billow Mechanics. Radio Science 4 pp 1299 - 1308.

Scorer R.S., 1978 : Environmental Aerodynamics. Ellis Horwood Ltd., Chichester.

Strauch R.G., Frisch A.S. and Sweezy W.B., 1975 : Doppler radar measurements of turbulence, shear, and dissipation rates in a convective storm. Preprints 16th Radar Meteorology Conference. Houston. American Met. Soc., pp 83 - 88.

Trout D. and Panofsky H.A., 1969 : Energy dissipation near the Tropopause. Tellus 21 pp 355 - 358.

Watkins C.D., 1971 : High-power radar for meteorological studies in clear air. Proc. I.E.E. 118 pp 519 - 528.

Whyman A.J. and Parkes D.M., 1979 : Sensitive fine-resolution radar for atmospheric research. Unpublished Memo No. 3179. Royal Signals and Radar Establishment, Malvern, England.

FIGURE CAPTIONS

1 Vertical sections of the component of the wind from 330° in ms^{-1} Section (a) along 010° was obtained from routine radiosonde ascents at 12 GMT plus one at Defford. Section (b) was obtained from a time sequence of ascents from Defford, the equivalent distance scale being obtained using the speed of travel, 12.7 ms^{-1}, of the synoptic scale pattern. Section (b) also shows the location of the observed billow event (wavey line) and the extent of the cloud deck (shown stippled) near the top of which the billows were observed.

2 Vertical profiles of the vertical gradient of dry bulb potential temperature, vertical wind shear and Richardson Number evaluated over layers 430 m deep from the radiosonde launched from Defford at 1450 GMT. The wavey line indicates the amplitude of the wave disturbance and the dot-dash lines show the levels at which the amplitude of the disturbance fell to one half its maximum value.

3 Time-range photographic chart of the intensity of the returned signal, which at a given range is proportional to the target reflectivity (η). The darker the chart the larger the signal intensity. The chart shows streamers of ice crystals near the top of a cirrus cloud deck, the slope of the streamers being modulated by a wave disturbance. The range scale is labelled in terms of both the range along the beam axis and of true altitude, allowing for the 60° elevation of the radar beam.

4 Time-range plot showing contours of radial velocity, V_r ($m\ s^{-1}$), along the radar beam elevated 60° above horizontal. The ordinate is labelled in terms of both range along the beam axis and true height. The abscissa is labelled in terms of both time and an equivalent distance assuming steady state conditions and a pattern velocity of 26 ms^{-1}. Each minute of data is derived from a 30 by 20 array consisting of radial velocity at 30 m intervals of range and at 3 second intervals of time.

5 Time-range plot showing contours of total radial velocity variance, σ_v^2 ($m^2\ s^{-2}$). Other details are as for Figure 4.

6 Time-range plot showing contours of radial shear, $\frac{\Delta Vr}{\Delta_r}$ (ms^{-1} per 60 m) evaluated as the difference in radial velocity between range gates whose midpoints were 60 m apart. The dashed line indicates a layer of reversed shear. Other details are as for Figure 4.

7a. Range-time chart of the intensity of the returned signal repeated from portion of Figure 3.

b. True height-time representation of streamlines associated with the primary billow disturbance. The streamline labelled (1) corresponds to the layer of reversed shear, the line labelled (2) is the axis of maximum shear; all other lines were derived from the shape of the ice crystal trails after making due allowance for their average slope.

c. True height-time representation of the vertical shear of the horizontal wind and variance due to turbulence, σ^2_{TURB}. The computed vertical shear was rather noisy and the raw data were smoothed with a 9 point filter to give the result shown above.

8 Detailed power spectra for the region enclosed by the small rectangle in Figures 7(b) and 7(c). Each box represents the velocity-power spectrum for a period of 1 second within a 30 m range gate. A horizontal displacement of one box represents 3 seconds which may be considered as equivalent to a horizontal distance of 78 m. Within a box the vertical power scale is linear and the horizontal scale covers values of Doppler velocity ranging from 10 ms^{-1} (lhs) to 15 ms^{-1} (rhs).

9 Detailed structure of the secondary billow within the small rectangle in Figs 7(b) and 7(c) constructed from arrays of 54 points (6 horizontally by 9 vertically) with effective resolutions of about 30 m vertically and 78 m horizontally. Fig 9(a) shows contours of radial velocity V_r in ms^{-1}; 9(b) shows contours of vertical velocity w (ms^{-1}) calculated using the two dimensional equation of continuity; 9(c) is the suggested flow pattern relative to the moving billows within this region; and 9(d) shows contours of the variance due to turbulence σ^2_{TURB} (m^2s^{-2}).

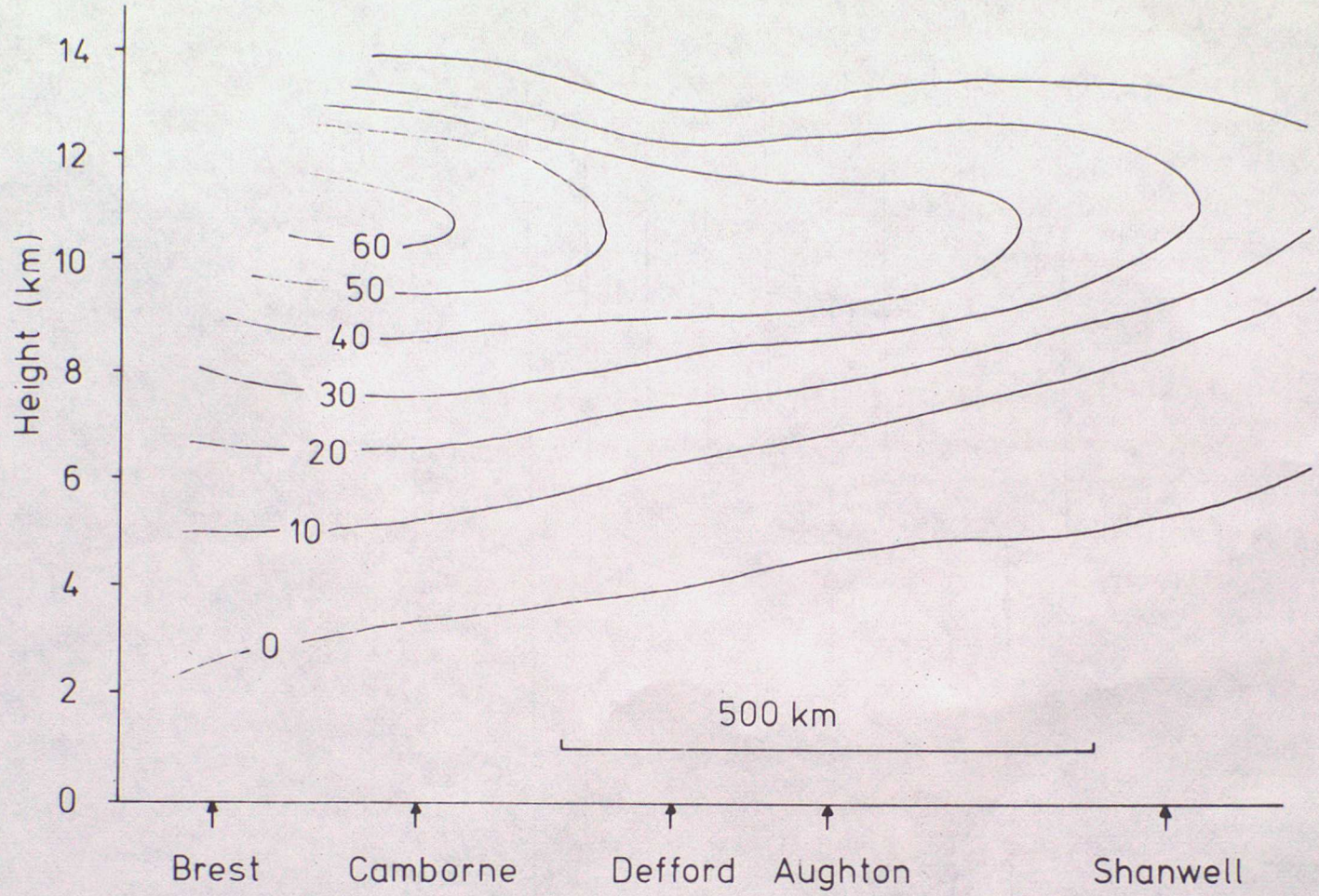
Height (km)
14
12
10
8
6
4
2
0
60
50
40
30
20
10
0
500 km
Brest
Camborne
Defford
Aughton
Shanwell

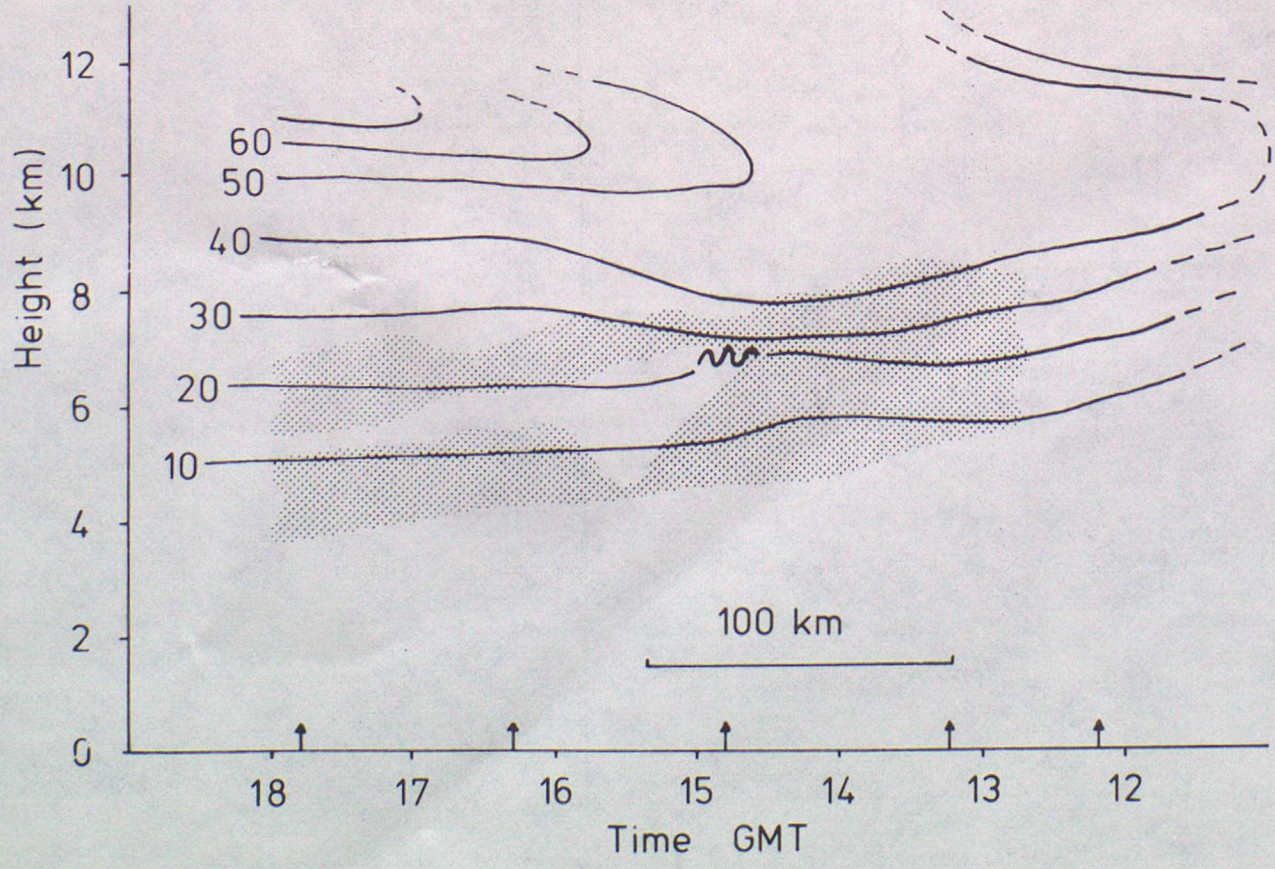
Height (km)
12
10
8
6
4
2
0
60
50
40
30
20
10
100 km
18
17
16
15
14
13
12
Time GMT

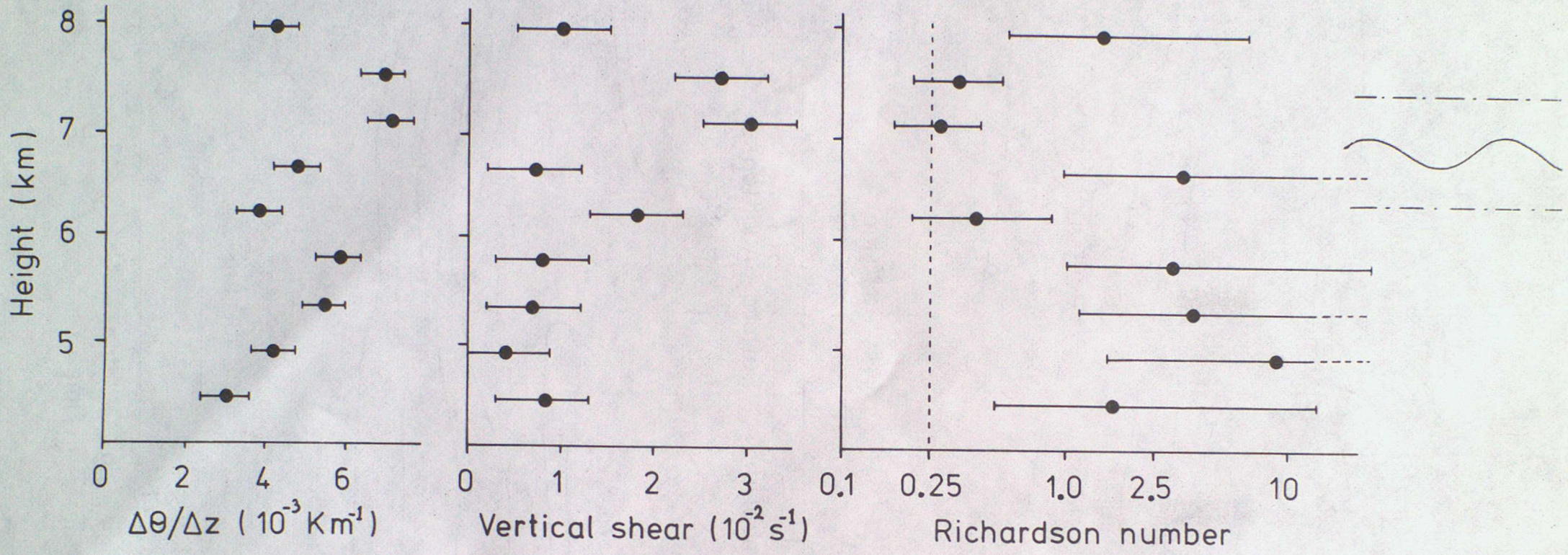
Height (km)
8
7
6
5
0
2
4
6
Δθ/Δz (10⁻³ Km⁻¹)
0
1
2
3
Vertical shear (10⁻² s⁻¹)
0.1
0.25
1.0
2.5
10
Richardson number

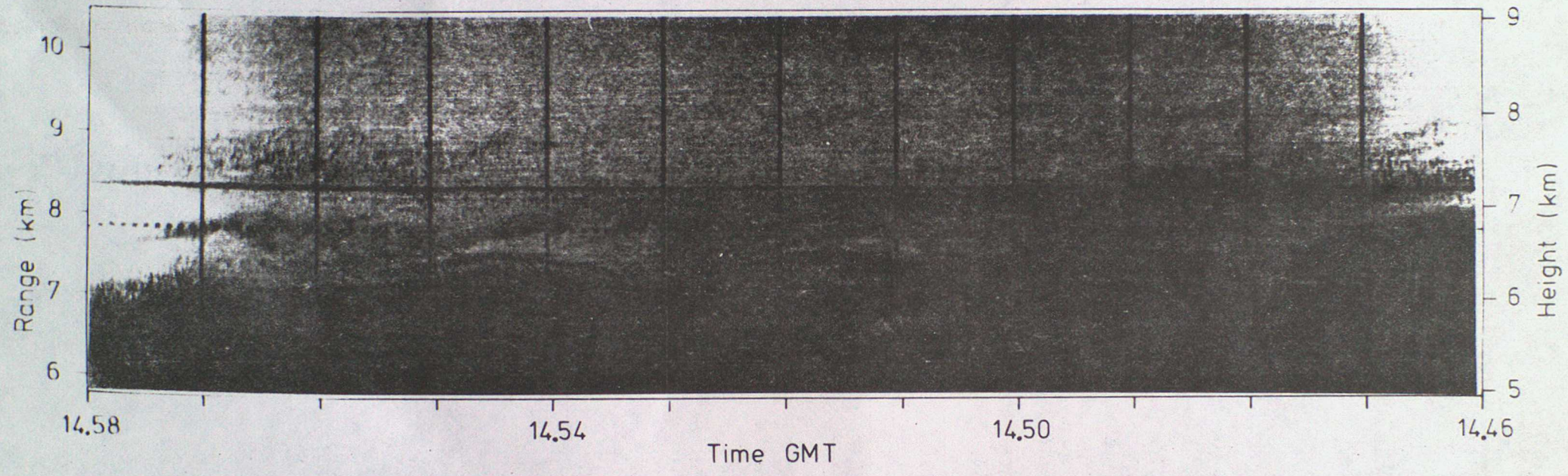
10
9
8
7
6
Range (km)
9
8
7
6
5
Height (km)
14.58
14.54
14.50
14.46
Time GMT

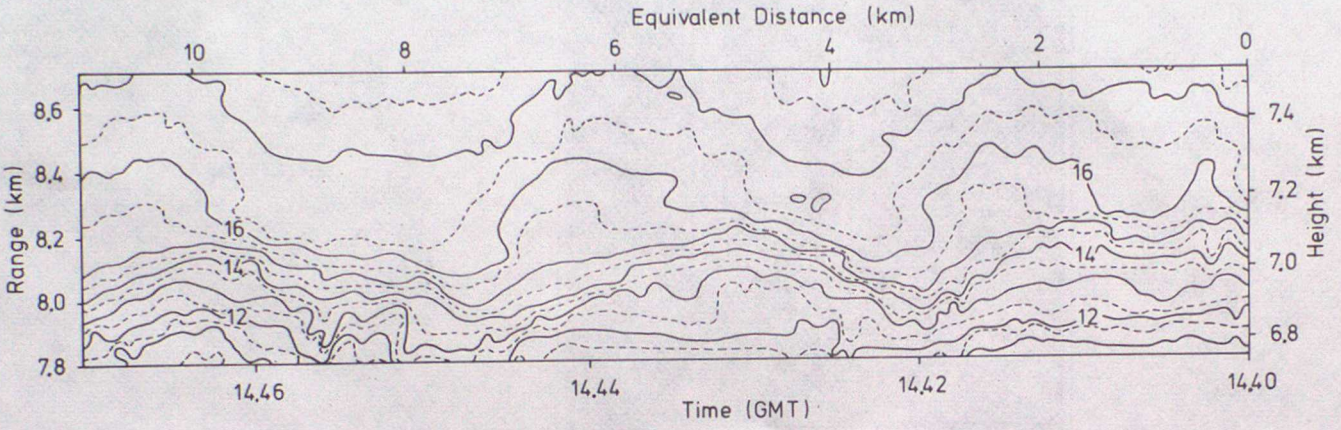
Equivalent Distance (km)
10
8
6
4
2
0
Range (km)
8.6
8.4
8.2
8.0
7.8
Height (km)
7.4
7.2
7.0
6.8
16
14
12
14.46
14.44
14.42
14.40
Time (GMT)

4a

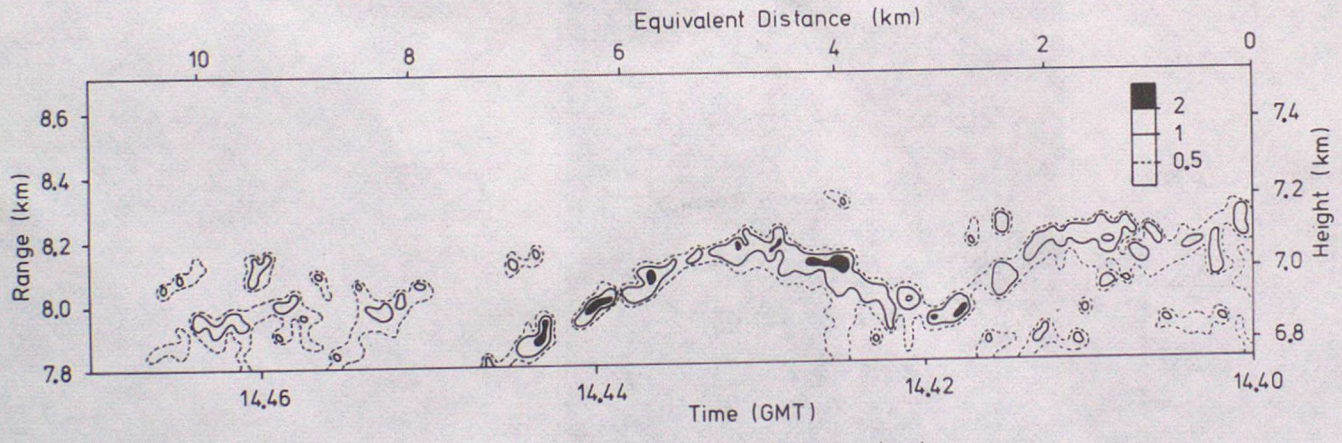
Equivalent Distance (km)
10
8
6
4
2
0
Range (km)
8.6
8.4
8.2
8.0
7.8
Height (km)
7.4
7.2
7.0
6.8
2
1
0.5
14.46
14.44
14.42
14.40
Time (GMT)

5a

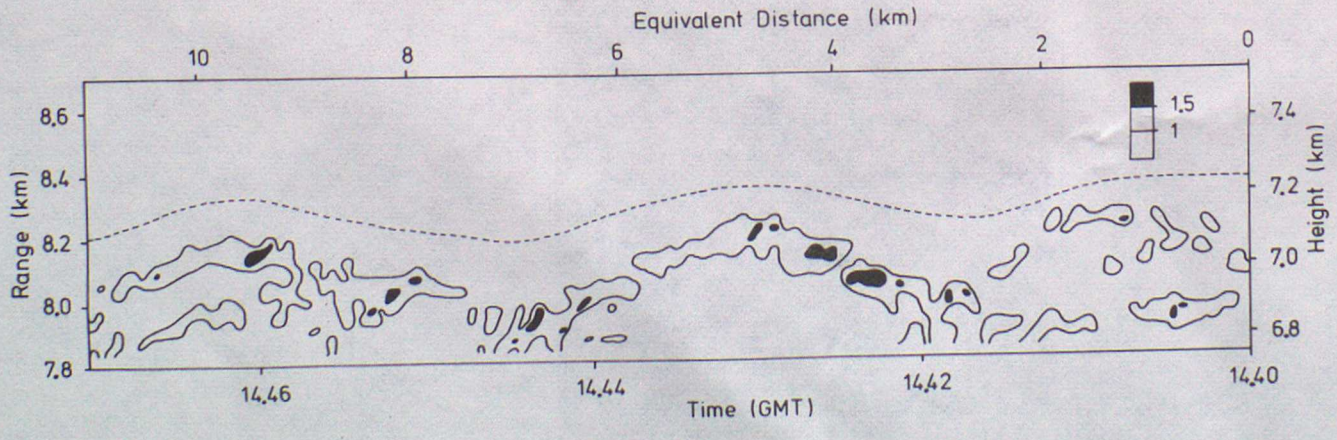
Equivalent Distance (km)
10
8
6
4
2
0
Range (km)
8.6
8.4
8.2
8.0
7.8
Height (km)
7.4
7.2
7.0
6.8
1.5
1
14.46
14.44
14.42
14.40
Time (GMT)

6a

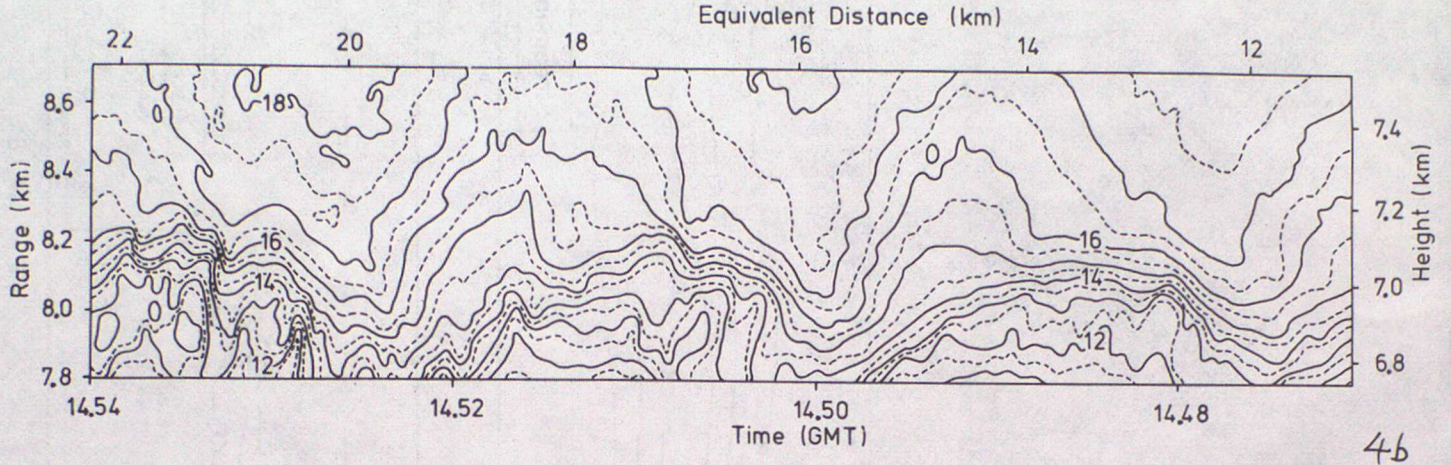
Equivalent Distance (km)
22
20
18
16
14
12
Range (km)
8.6
8.4
8.2
8.0
7.8
Height (km)
7.4
7.2
7.0
6.8
18
16
14
12
14.54
14.52
14.50
14.48
Time (GMT)

4b

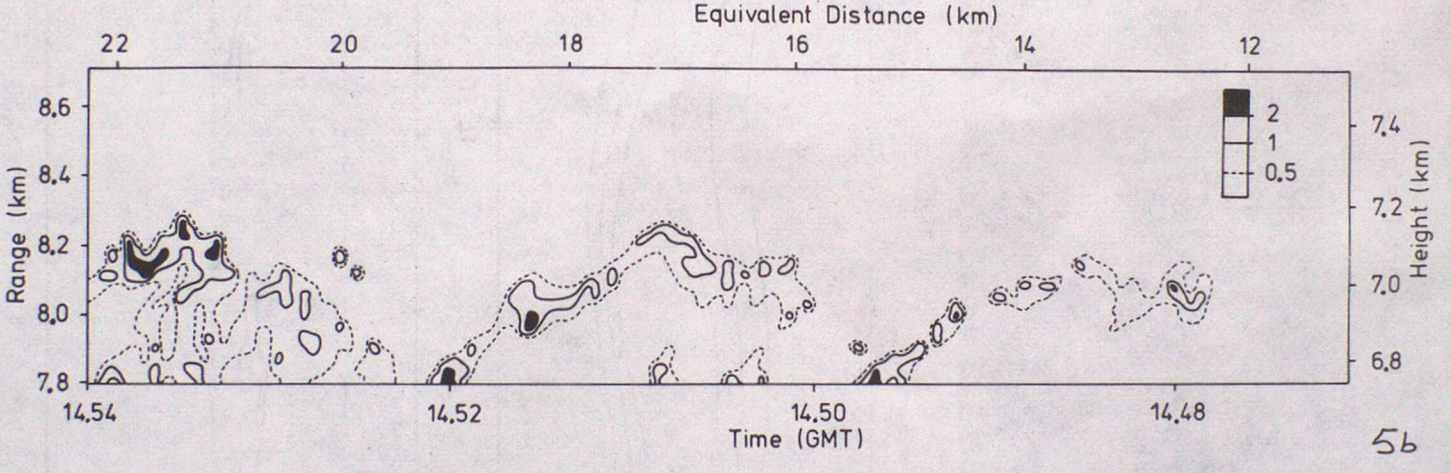
Equivalent Distance (km)
22
20
18
16
14
12
Range (km)
8.6
8.4
8.2
8.0
7.8
Height (km)
7.4
7.2
7.0
6.8
2
1
0.5
14.54
14.52
14.50
14.48
Time (GMT)

5b

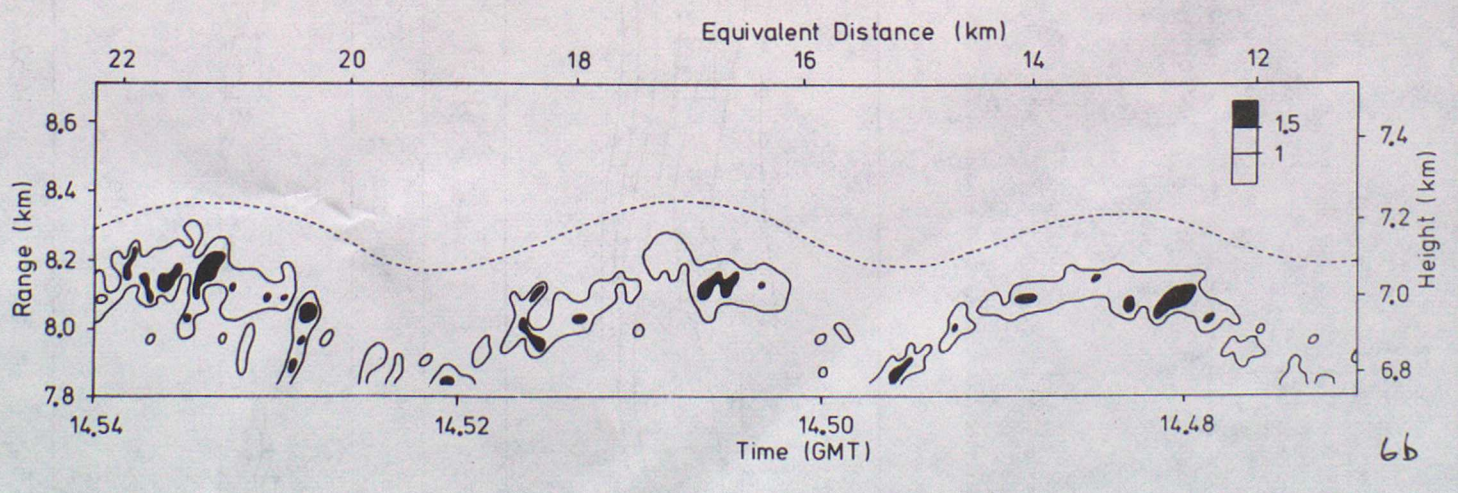
Equivalent Distance (km)
22
20
18
16
14
12
Range (km)
8.6
8.4
8.2
8.0
7.8
Height (km)
7.4
7.2
7.0
6.8
1.5
1
14.54
14.52
14.50
14.48
Time (GMT)

6b

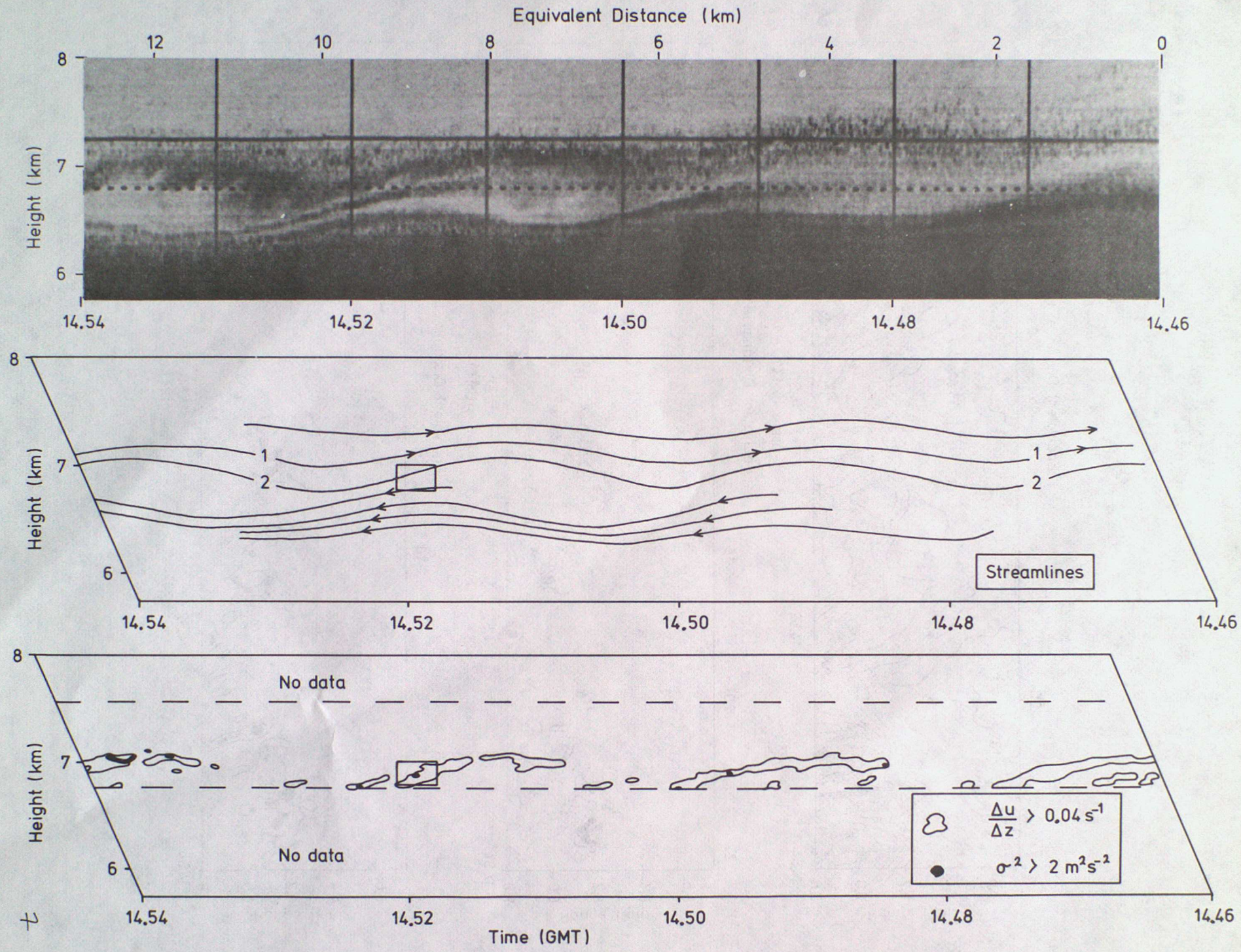
Equivalent Distance (km)
12
10
8
6
4
2
0
8
7
6
Height (km)
14.54
14.52
14.50
14.48
14.46
1
2
Streamlines
No data
No data
$\frac{\Delta u}{\Delta z} > 0.04\ s^{-1}$
$\sigma^2 > 2\ m^2 s^{-2}$
Time (GMT)

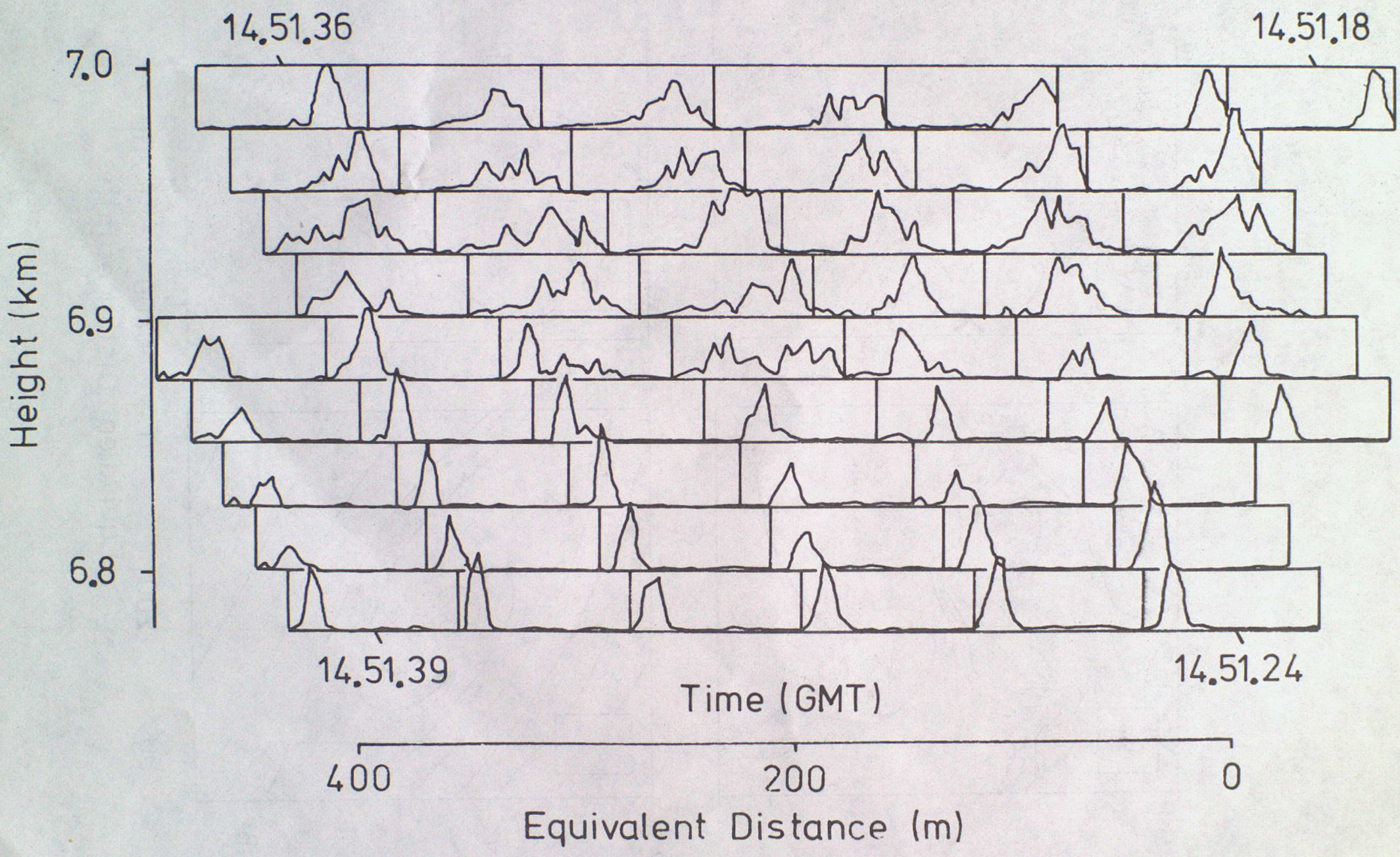
14.51.36
14.51.18
7.0
6.9
6.8
Height (km)
14.51.39
14.51.24
Time (GMT)
400
200
0
Equivalent Distance (m)

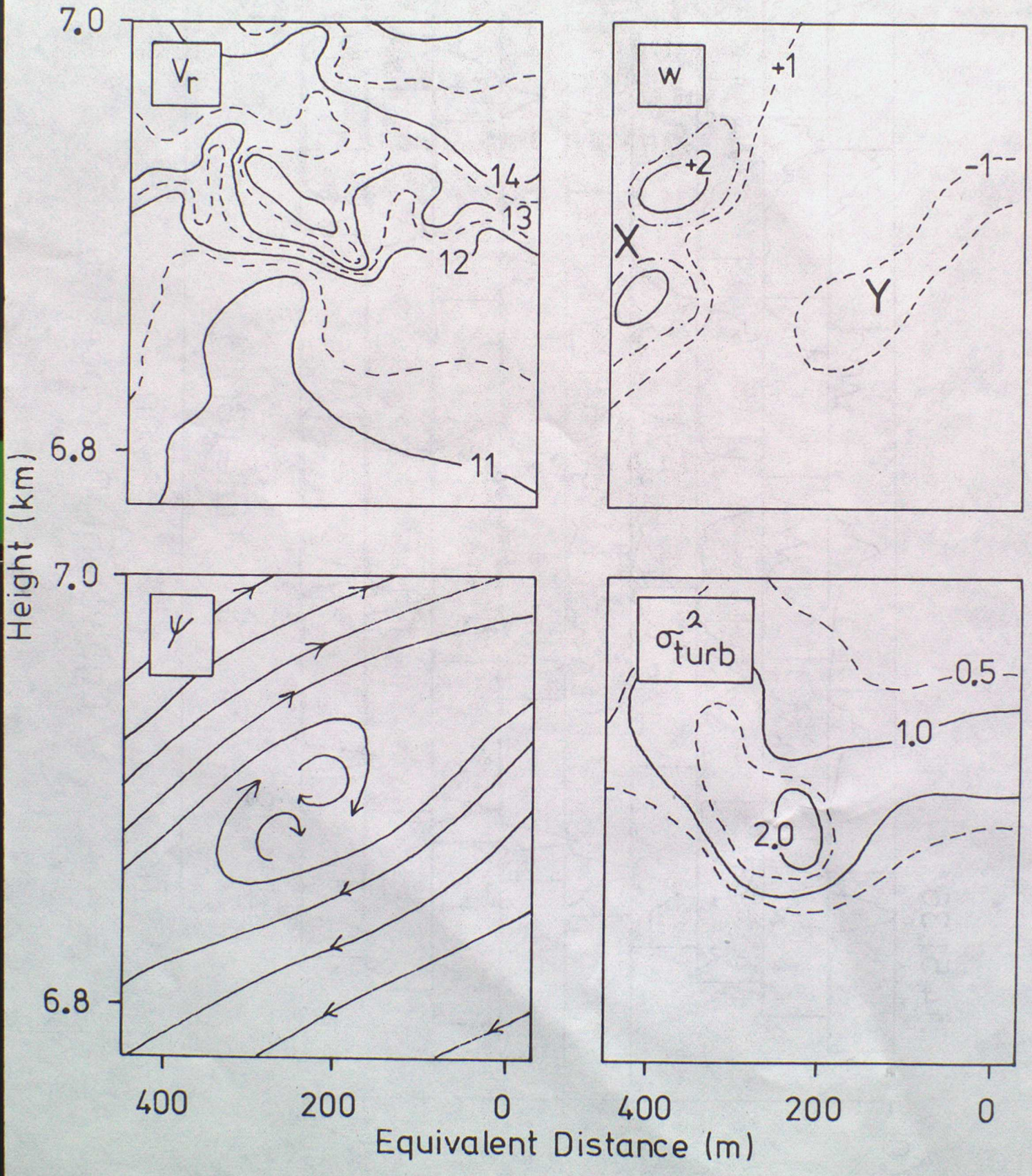
7.0
6.8
V_r
14
13
12
11
w
+1
+2
-1
X
Y
7.0
6.8
Ψ
σ^2_{turb}
0.5
1.0
2.0
400
200
0
400
200
0
Height (km)
Equivalent Distance (m)

METEOROLOGICAL OFFICE RADAR RESEARCH LABORATORY - MET O RRL

Research Reports

No 1 The Short Period Weather Forecasting Pilot Project
K A Browning

No 2 Observation of Strong Wind Shear using Pulse Compression Radar.
K A Browning, P K James (Met O RRL). D M Parkes, C Rowley A J Whyman (RSRE)

No 3 Assessment of a Real-Time Method for Reducing the Errors in Radar Rainfall Measurements due to Bright-Band
J L Clarke, RSRE, C G Collier, Met O RRL

No 4 Meteorological Applications of Radar
K A Browning

No 5 Structure of the Lower Atmosphere Associated with Heavy Falls of Orographic Rain in South Wales.
J Nash, K A Browning

No 6 On the Benefits of Improved Short Period Forecasts of Precipitation to the United Kingdom - Non Military Applications Only
C G Collier

No 7 Persistence and Orographic Modulation of Mesoscale Precipitation Areas in a Potentially Unstable Warm Sector.
F F Hill, K A Browning

No 8 Mesoscale Structure of Line Convection at Surface Cold Fronts.
P K James, K A Browning

No 9 Objective Forecasting Using Radar Data: A Review
C G Collier

No 10 Structure, Mechanism and Prediction of Orographically Enhanced Rain in Britain: A Review
K A Browning

No 11 A Strategy for Using Radar & Satellite Imagery for Very-Short-Range Precipitation Forecasting.
K A Browning, C G Collier, P Menmuir.

No 12 Radar as part of an Integrated System for Measuring and Forecasting Rain in the UK: Progress and Plans.
K A Browning

No. 13 Data Processing in the Meteorological Office Short-Period Weather Forecasting Pilot Project.
C G Collier

No.14 Severe Wintertime Hailstorm in South Devon
R G Owens

No.15 Radar Observations of the Troposphere in Clear Air Conditions.
P K James

No.16 Local Weather Forecasting (Text of a review lecture presented at the Royal Society)
K A Browning

No.17 An Observational Study of Primary & Secondary Billows in the Free Atmosphere.
P K James, K A Browning

No.18 The Production, in Real Time, of a Rainfall Field Covering a Large Area using Data from Several Weather Radars.
P R Larke, C G Collier.